Research Square

Preprints are preliminary reports that have not undergone peer review.
They should not be considered conclusive, used to inform clinical practice,
or referenced by the media as validated information.

Runoff Interception Characteristics of a Y-Shaped Bamboo Structure for Slope Protection

Xiaojuan Yu
Yancheng Institute of Technology
Qingjian Li
Yancheng Institute of Technology
Wenyan Xu
Jiangsu Port and Shipping Investment Development Co., Ltd
Zhizhong Chen
Jiangsu Provincial Transportation Engineering Group Co., Ltd
Chao Liu
liuchaodeer@ycit.edu.cn
Yancheng Institute of Technology
Chao Chen
Yancheng Keheng Land Surveying Co., Ltd

Article

Keywords: Ecological slope protection, Y-shaped bamboo structure, surface runoff, intercepted runoff mass, theoretical model

Posted Date: October 29th, 2026

DOI: https://doi.org/10.21203/rs.3.rs-11203973/v1

License: This work is licensed under a Creative Commons Attribution 4.0 International License.
Read Full License

Additional Declarations: No competing interests reported.

Article

Runoff Interception Characteristics of a Y-Shaped Bamboo Structure for Slope Protection

Xiaojuan Yu [1], Qingjian Li [1], Wenyan Xu [2], Zhizhong Chen [3], Chao Liu [1,*] and Chao Chen [4]

[1] School of Civil Engineering, Yancheng Institute of Technology, Yancheng 224005, China; yuxiaojuan@ycit.edu.cn (X.Y.); lqj88h@163.com (Q.L.)
[2] Jiangsu Port and Shipping Investment Development Co., Ltd, Nanjing 211000, China; 501351332@qq.com
[3] Jiangsu Provincial Transportation Engineering Group Co., Ltd., Xiangshui Branch, Yancheng, 224600, China; 18755893989@163.com
[4] Yancheng Keheng Land Surveying Co., Ltd., Yancheng, 224007, China; chenchao202609@126.com
* Correspondence: liuchaodeer@ycit.edu.cn

Abstract: Conventional slope protection systems are susceptible to runoff-induced erosion, surface-soil loss, and shallow soil deformation under rainfall conditions. This study developed a Y-shaped bamboo structure integrating runoff interception and seepage drainage functions. Model tests and theoretical analysis were conducted to investigate the runoff interception efficiency of the structure under simulated rainfall conditions. The results showed that the Y-shaped bamboo structure exhibited effective runoff interception performance, with the cumulative intercepted runoff increasing approximately linearly with rainfall duration. The included angle between the two wings had the greatest effect on runoff interception efficiency, followed by wing length and wing diameter, with these three parameters collectively accounting for 93.04% of the total variance. Furthermore, a theoretical runoff interception model coupling weir flow theory with Darcy's law was developed and validated against laboratory model tests, showing good agreement with the experimental results. The findings provide a theoretical basis for geometric optimization and support the potential application of Y-shaped bamboo structures in ecological slope protection.

Keywords: Ecological slope protection; Y-shaped bamboo structure; surface runoff; intercepted runoff mass; theoretical model

1. Introduction

Rainfall-induced erosion is an important factor affecting the long-term stability of slopes [1–3]. Rainfall infiltration increases soil water content and pore-water pressure, thereby reducing the shear strength of shallow soil layers and potentially causing surface deformation, failure of protective layers, and even shallow landslides [4–7]. Such rainfall-induced hazards can have severe consequences. For example, intense rainfall in Wanzhou, China, in July 2023 triggered landslides and other geological disasters, resulting in 17 deaths [8]. These events highlight the need for effective slope protection measures to intercept rainfall runoff and mitigate its erosive effects and the adverse effects of rainfall infiltration.

Various techniques have been developed to mitigate rainfall-induced slope erosion, including runoff interception, subsurface drainage, and surface protection. Runoff interception measures, such as straw check dams and sandbag barriers, are designed to intercept concentrated flow, reduce flow velocity, and promote sediment deposition [9–13]. Donald et al. [12] demonstrated that straw barriers could effectively reduce peak runoff discharge and flow velocity while enhancing sediment retention, with their performance being strongly influenced by porosity, compaction, and flexibility. Robichaud et al. [13] further showed that contour-aligned straw barriers could effectively intercept concentrated runoff and promote sediment deposition. Subsurface drainage provides another means of mitigating the effects of rainfall infiltration by facilitating the removal of infiltrated water and reducing pore-water pressure. Drainage systems incorporating PVC or HDPE pipes and straw blind drains have been employed to improve subsurface drainage conditions and enhance slope stability [14–15]. Zhang et al. [16] reported that appropriately configured drainage channels could promote the drainage of infiltrated water, reduce water accumulation and pore-water pressure buildup, and consequently mitigate rainfall-induced slope deformation. Surface protection measures, including straw mats and erosion-control blankets, primarily increase surface roughness, attenuate raindrop impact, and reduce runoff velocity, thereby limiting soil detachment and sediment transport [17–19]. Chulhee Won et al. [20] investigated the use of straw mats for runoff and sediment control and found that they substantially reduced sediment loss and runoff turbidity under different coverage conditions. Although these approaches have proven effective, they generally focus on different

aspects of rainfall-induced slope erosion. Runoff interception primarily regulates overland flow, subsurface drainage controls water accumulation within the soil, and surface protection shields the soil surface from direct rainfall and runoff action. Therefore, individual measures generally have limited ability to simultaneously provide runoff interception, flow diversion, energy dissipation, and drainage. This limitation is particularly important under intense rainfall, when surface runoff and rainfall infiltration occur simultaneously and interact with each other. An integrated protection system that can coordinate these functions is therefore desirable.

In this study, an integrated Y-shaped bamboo structure is proposed, consisting of two inclined wings that intercept overland flow and a central drainage stem that drains captured runoff into the subsoil. Laboratory rainfall erosion model tests were conducted to evaluate its hydraulic performance. A theoretical model was further developed to predict runoff interception performance by coupling weir flow theory with Darcy's law. The results provide a basis for geometric optimization and theoretical prediction of runoff interception performance, as well as for assessing the potential application of the proposed structure in rainfall-induced slope erosion control.

2. Experimental program and methodology

2.1. Design and fabrication of Y-shaped bamboo structure

The Y-shaped bamboo structure was designed as an integrated structural unit to provide runoff interception, flow diversion, energy dissipation, and drainage. The two inclined wings were designed to intercept and redirect concentrated runoff, thereby reducing flow velocity and dissipating hydraulic energy before the runoff continued downslope. The central drainage stem was embedded into the soil to provide mechanical restraint through soil-bamboo interaction. The natural gaps between the bamboo elements may also provide preferential pathways for local water drainage.

Based on this design concept, the structure was fabricated using bamboo culms assembled into bundles and vegetation-bag fabric. The bamboo culms were first cut to the specified dimensions and assembled into a Y-shaped configuration consisting of one central drainage stem and two inclined wings. The specific geometric parameters, including wing diameter, wing length, and included angle, were varied systematically as described in Section 2.3. The assembled bamboo framework was then wrapped with a single layer of polypropylene nonwoven vegetation-bag fabric to form an integrated structural component. No metal nails or other rigid fasteners were used at the joints, which avoided potential joint loosening associated with corrosion. The final configuration of the Y-shaped bamboo structure is shown in Figure 1.

2.2. Raw materials

The bamboo used in this study was supplied by a commercial manufacturer. The culms were approximately one year old, and the specimens were obtained from internodal sections in the middle portion of the culms, approximately 1-3 m above the base. The bamboo has an average outer diameter of 1.0 cm and an average wall thickness of 1.5 mm. At a moisture content of 12%, the bamboo has an average density of 0.68 g/cm3, a mean longitudinal compressive strength of 67.6 MPa, and a longitudinal shear strength of 11.1 MPa. For comparison, a solid-wood structure was also prepared (see Section 2.3). The solid-wood structure was fabricated from pine (Pinus spp.) with the same external geometry as the bamboo structure. At 12% moisture content, the pine has an average density of 0.55 g/cm3. Both bamboo and wood specimens were conditioned to 12% moisture content and left uncoated to maintain their natural surface conditions. The vegetation bags were made of polypropylene nonwoven vegetation bag fabric, with an areal mass of 150 g/m² and a measured thickness of 0.86 mm. The saturated hydraulic conductivity and effective porosity of the fabric are 0.042 cm/s and approximately 0.75, respectively.

2.3. Experimental apparatus and slope model configuration

Indoor runoff interception tests under simulated rainfall were conducted in a transparent acrylic flume measuring 70 cm × 70 cm × 70 cm (Figure 1). The transparent sidewalls enabled direct observation of runoff generation and flow development during rainfall. An impermeable acrylic slope model with a gradient of 1:2.5 was installed inside the flume, with an effective slope length of approximately 65 cm. A drainage space was provided at the slope toe to facilitate collection and discharge of surface runoff. The Y-shaped structure was placed centrally on the slope surface, maintaining a minimum clearance of 10 cm from the flume sidewalls to minimize boundary effects. The slope surface was impermeable, resulting in a runoff coefficient approaching unity. This configuration minimized the influences of soil infiltration and surface roughness, allowing the runoff interception performance of the bamboo structure to be evaluated under controlled conditions.

The Y-shaped bamboo structure was installed at designated positions on the slope, with the two wings extending along the slope surface. For comparison, a Y-shaped solid-wood structure with the same geometric configuration and dimensions was also tested under identical conditions. In terms of the hydrological pathway, runoff captured by the two inclined wings was guided by gravity towards the central junction and subsequently discharged through the hollow central drainage stem into the central collection container. Conversely, any runoff not intercepted by the structure flowed directly down the impermeable slope surface and was collected in the two side containers. A rainfall simulator, consisting of a steel support frame and a sprinkler network, was mounted above the flume. The sprinkler heads were spaced 30 cm apart, and the water-supply pressure was adjusted to maintain a constant rainfall intensity of 60 mm/h. This intensity was selected based on the local 10-year return-period rainfall intensity. Prior to each test, the actual rainfall intensity was verified using a standard rain gauge to ensure consistency with the target value. Three collection containers were positioned beneath the flume outlet. A runoff separation channel at the base of the model divided the collected water according to its flow path: the two side containers collected surface runoff flowing directly from the slope, whereas the central container collected water discharged through the lower end of the central drainage stem. Each container was placed on an electronic balance, and the mass of collected water was recorded at 2-min intervals.

To systematically evaluate the effects of wing geometry, three parameters were varied: wing diameter, wing length, and included angle. The wing length, included angle, and wing diameter were set at 20, 30, and 40 cm; 60°, 80°, 100°, and 120°; and 2, 3, 4, and 5 cm, respectively, resulting in 48 experimental combinations. Each combination was tested in triplicate, and the average values were used for subsequent analysis. The relative standard deviation among the three replicates was consistently below 5%, indicating satisfactory experimental reproducibility.

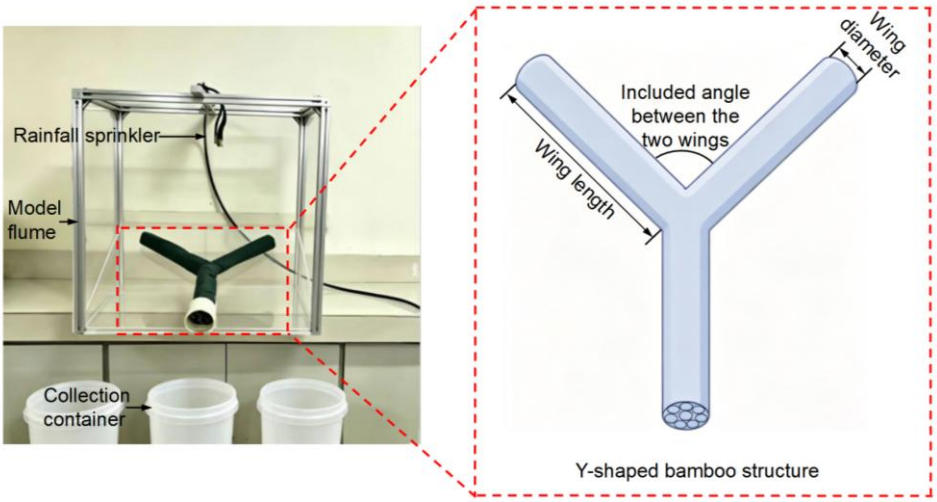


Figure 1. Indoor runoff interception test.

2.4. Experimental results

2.4.1 Effect of wing diameter

Figure 2 shows the effect of wing diameter on intercepted runoff mass. At a constant wing length of 20 cm and an included angle of 80°, both the Y-shaped bamboo structure and the Y-shaped solid-wood structure exhibited an approximately linear increase in intercepted runoff mass with rainfall duration. The runoff interception efficiency was defined as the proportion of total surface runoff that was captured by the structure and discharged through the central drainage stem. For the Y-shaped solid-wood structure with wing diameters of 2, 3, 4, and 5 cm, the final intercepted runoff masses were 1.00, 1.10, 1.15, and 1.25 kg, corresponding to interception efficiencies of 15.38%, 16.92%, 17.69%, and 19.23%, respectively. The Y-shaped bamboo structure intercepted 1.20, 1.25, 1.50, and 1.65 kg, achieving interception efficiencies of 18.46%, 19.23%, 23.08%, and 25.38%, respectively. These interception efficiencies represent increases of 20.00%, 13.65%, 30.47%, and 31.98%, respectively, relative to the corresponding Y-shaped solid-wood structure. Increasing the wing diameter consistently improves runoff interception efficiency for both structures. This improvement is likely related to the increased transverse structural scale of the wings, which enhances their capacity to intercept and convey approaching runoff toward the central junction. A larger wing diameter also provides a greater internal space within the bamboo bundle, potentially allowing more runoff to enter and pass through the structure before discharge

through the central drainage stem. The Y-shaped bamboo structure consistently exhibits higher runoff interception efficiency than the Y-shaped solid-wood structure at all tested wing diameters, which may be attributed to its tubular configuration and associated internal flow pathways. These results indicate that wing diameter primarily influences the interception and conveyance capacity of the structure.

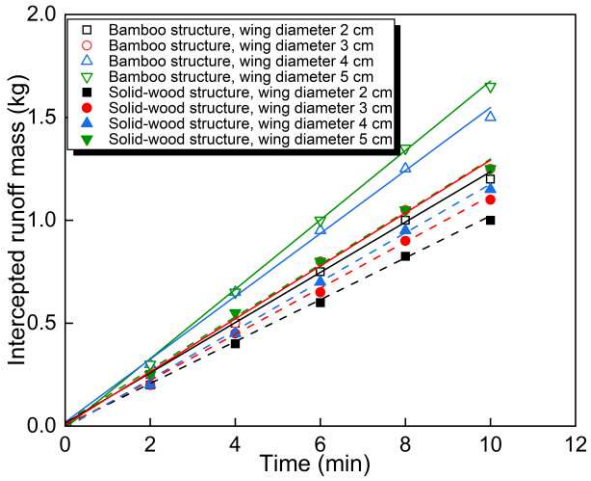


Figure 2. Effect of wing diameter on intercepted runoff mass.

2.4.2 Effect of included angle

Figure 3 shows the effect of the included angle on intercepted runoff mass. As the included angle increased from 60° to 80°, 100°, and 120°, the final intercepted runoff mass of the Y-shaped solid-wood structure increased from 0.80 to 1.00, 1.15, and 1.25 kg, corresponding to interception efficiencies of 12.31%, 15.38%, 17.69%, and 19.23%, respectively. For the Y-shaped bamboo structure, the corresponding intercepted runoff masses were 0.95, 1.20, 1.25, and 1.35 kg, with interception efficiencies of 14.62%, 18.46%, 19.23%, and 20.77%, respectively. Increasing the included angle progressively improves runoff interception efficiency for both structures. Unlike wing diameter, which primarily changes the transverse structural scale, the included angle controls the spatial orientation of the two wings and the direction of intercepted runoff toward the central junction. The Y-shaped bamboo structure consistently exhibits higher runoff interception efficiency than the Y-shaped solid-wood structure across all tested included angles, indicating a persistent interception advantage over the tested angle range. These results suggest that the included angle primarily governs the convergence and redistribution of intercepted runoff within the Y-shaped structure.

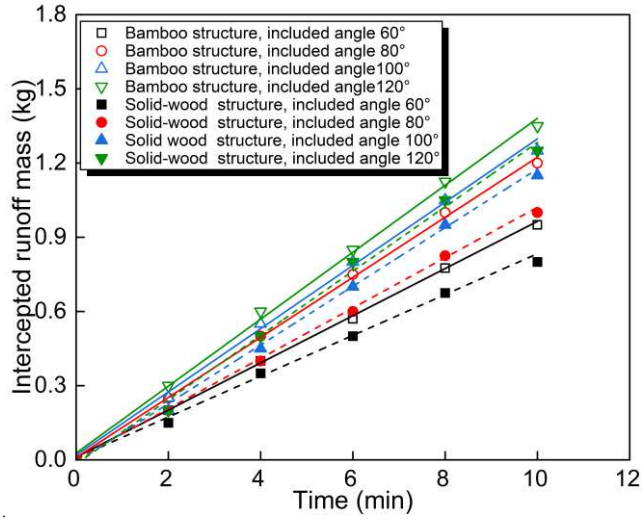


Figure 3. Effect of the included angle on intercepted runoff mass.

2.4.3 Effect of wing length

Figure 4 shows the effect of wing length on intercepted runoff mass and runoff interception efficiency. With the wing diameter and included angle fixed at 2 cm and 60°, respectively, the final intercepted runoff mass of the Y-shaped bamboo structure increased from 0.95 to 1.25 kg as the wing length increased from 20 to 40 cm, corresponding to an increase in interception efficiency from 14.62% to 19.23%. Under the same geometric conditions, the Y-shaped solid-wood structure showed a smaller increase, from 0.80 to 1.05 kg, with interception efficiency rising from 12.31% to 16.15%. The difference in intercepted runoff mass between the Y-shaped bamboo structure and the Y-shaped solid-wood structure increased from 0.15 kg at 20 cm to 0.20 kg at 40 cm. Increasing the wing length progressively improves runoff interception efficiency for both structures. Unlike wing diameter, which primarily changes the transverse structural scale, wing length primarily governs the interception area and contact length along the slope, thereby influencing the total amount of runoff that can be captured. A longer wing likely extends the transverse coverage of the structure, allowing it to intercept runoff from a wider flow section. The Y-shaped bamboo structure consistently exhibits higher runoff interception efficiency than the Y-shaped solid-wood structure across all tested wing lengths, indicating a persistent interception advantage over the tested length range. These results suggest that wing length primarily influences the capture area and interception capacity of the structure.

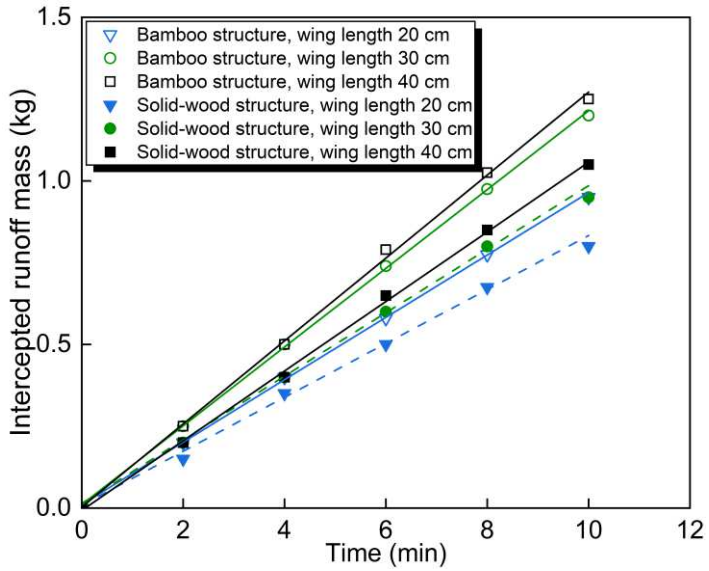


Figure 4. Rainfall collection performance of the structure under varying wing lengths.

2.4.4 Sensitivity analysis

To quantify the relative importance of the three geometric parameters, a sensitivity analysis was conducted using the 10-min intercepted runoff mass as the response variable. The 10-min value refers to the cumulative amount of runoff collected at the end of each 10-min test run, which is equivalent to the final intercepted runoff mass reported in Sections 2.4.1–2.4.3. Table 1 summarizes the range analysis results for the effects of the three geometric parameters on the 10-min intercepted runoff mass under different parameter combinations. The range analysis indicated that the sensitivity ranking of the parameters followed the order of included angle > wing length > wing diameter. Notably, the mean range of the included angle was 2.53 times that of wing diameter, indicating that the 10-min intercepted runoff mass is more sensitive to changes in the included angle than to changes in wing diameter. The wing length exhibits the largest standard deviation among the three parameters, indicating greater variability in its sensitivity across different experimental conditions. In contrast, wing diameter shows the lowest mean range and standard deviation, reflecting a relatively weak and stable influence. Overall, the range analysis identified the included angle as the most sensitive parameter, followed by wing length, whereas wing diameter shows the weakest influence.

Table 2 presents the variance decomposition results based on analysis of variance (ANOVA). As shown in Table 2, the contribution percentages of the three main effects follow the same order: included angle (52.59%) > wing length (31.57%) > wing diameter (8.88%), which is consistent with the sensitivity ranking obtained from the range analysis. The three main effects collectively account for 93.04% of the total variance, indicating that the individual effects of the three geometric parameters dominate the variation in the 10-min intercepted runoff mass. The interaction effects collectively account for the remaining 6.96% of the total variance, with the wing length × included angle interaction contributing

5.18%, whereas the three interaction terms involving wing diameter collectively contribute only 1.78%. Wing diameter accounts for only 8.88% of the total variance, and its relatively small interaction contributions further indicate that wing diameter plays a comparatively limited role in the overall response. These results indicate that greater attention should be given to the included angle and wing length when optimizing runoff interception performance, whereas wing diameter exhibits a relatively weak and stable influence.

Table 1. Range analysis of intercepted runoff mass.

Parameter	Range (kg)	Mean range (kg)	Standard deviation (kg)	Sensitivity ranking
Included angle(θ)	0.350~0.950	0.7375	0.1949	1
Wing length (L_y)	0.250~0.850	0.5281	0.2038	2
Wing diameter (d_y)	0.150~ 0.450	0.2917	0.0954	3

* Sensitivity ranks are 1, 2, and 3 from most to least sensitive.

Table 2. ANOVA results and sensitivity analysis.

Factor	Sum of squares (SS)	Contribution (%)	Sensitivity ranking
θ（main effect of included angle）	3.6938	52.59%	1
L_y（main effect of wing length）	2.2176	31.57%	2
d_y（main effect of wing diameter）	0.6238	8.88%	3
$L_y \times \theta$（two-way interaction）	0.3641	5.18%	-
$L_y \times d_y \times \theta$（three-way interaction）	0.0676	0.96%	-
$L_y \times d_y$（two-way interaction）	0.0391	0.56%	-
$d_y \times \theta$ (two-way interaction)	0.0183	0.26%	-
Total SS	7.0242	100.00%	-

* Sensitivity ranks are 1, 2, and 3 from most to least sensitive.

3. Theoretical calculations

3.1 Model development

As illustrated in Figure 5, a Y-shaped bamboo structure model was established to characterize the processes of runoff interception, infiltration, and drainage. To simplify the theoretical analysis, the following assumptions were adopted:

(1) The rainfall intensity is uniformly distributed in both temporal and spatial domains;

(2) Water flow within the vegetation bag wall follows Darcy's law[21,22];

(3) The surface runoff film is treated as a laminar flow governed by the Nusselt film flow theory[23,24];

(4) The water heads at the junctions of the two wings are assumed to be equal, and the resulting ponding depth is limited by the height of the retaining bund;

(5) Water infiltrating into the bamboo bundle within the Y-shaped bamboo structure is assumed to drain entirely through the outlet at the bottom of the bundle, while the amount of water penetrating through the vegetation bag into the underlying soil is neglected.

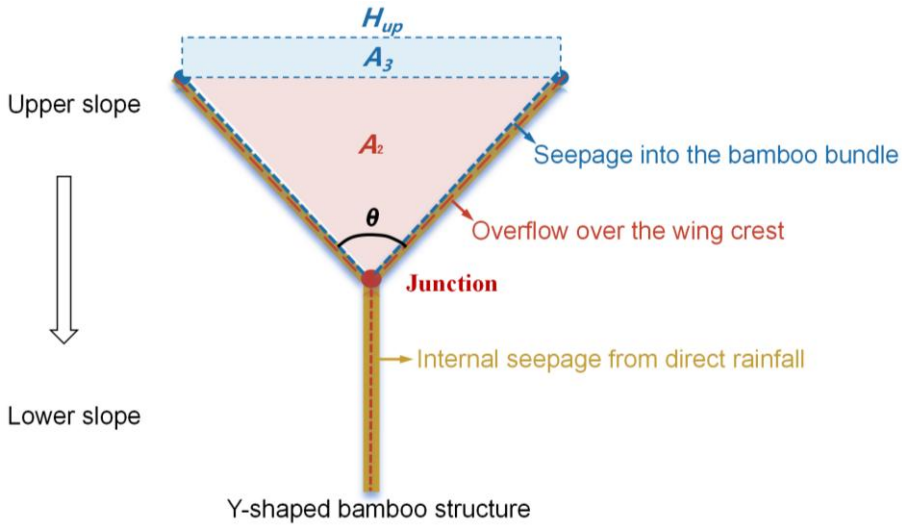


Figure 5. Schematic diagram of the Y-shaped bamboo structure model.

3.1.1 Geometry and contributing areas

The water-contributing areas associated with the Y-shaped bamboo structure were divided into two categories: the upslope surface area generating runoff and the projected area of the bamboo structure receiving direct rainfall. These two rainfall sources were treated separately to avoid double counting.

The triangular contributing area enclosed by the two wings, A2, is calculated as:

$$A_2 = \frac{1}{2} L_y{}^2 sin\theta \tag{1}$$

where, L_y is the wing length; θ is the included angle between the two wings.

The lateral spacing between the two wing tips, W_{tip}, is determined as:

$$W_{tip} = 2L_y sin\left(\frac{\theta}{2}\right) \tag{2}$$

The rectangular contributing area located upslope of the Y-shaped structure, A_3, is calculated as:

$$A_3 = W_{tip} H_{up} \tag{3}$$

where, H_{up} is the upslope contributing flow length.

Therefore, the total upslope contributing area generating surface runoff is:

$$A_c = A_2 + A_3 \tag{4}$$

The horizontal projected area of the Y-shaped bamboo structure is independently calculated as:

$$A_1 = L_s d_s \tag{5}$$

where, L_s is the length of the central drainage stem; d_s is the diameter of the central drainage stem. A_1 is used only to determine the rainfall directly received by the bamboo structure and is not included in A_c.

3.1.2 Rainfall input and unit wing-length inflow

Under a rainfall intensity I, the total runoff generated from the upslope contributing area is:

$$Q_{in,total} = IA_c \tag{6}$$

where, $Q_{in,total}$ is the total runoff inflow to the Y-shaped structure. For the laboratory model, infiltration and other rainfall losses from the upslope contributing surface are neglected.

The rainfall directly received by the bamboo structure is calculated as:

$$Q_{direct} = IA_1 \tag{7}$$

where, Q_{direct} is the direct rainfall input to the bamboo structure.

Assuming that the upslope runoff is symmetrically distributed between the two wings, the inflow rate per unit wing length is:

$$q'_{in} = \frac{Q_{in,total}}{2L_y} \tag{8}$$

where, q'_{in} is the runoff inflow rate per unit wing length. This assumption represents the average inflow condition along the two wings in the laboratory model. It should be noted that $Q_{in,total}$ and Q_{direct} represent two independent rainfall inputs. The former is generated by the upslope contributing surface, whereas the latter falls directly onto the bamboo structure.

3.1.3 Water balance and overflow over the wing crest

As runoff reaches the vegetation bag wall along each bamboo wing, the incoming water is partitioned into transverse seepage through the bag wall and overflow over the wing crest. Under quasi-steady conditions, the water balance per unit wing length is expressed as:

$$q'_{in} = q_0 + q'_{over} \tag{9}$$

where, q_0 is the transverse seepage rate through the vegetation bag wall per unit wing length; q'_{over} is the overflow discharge per unit wing length.

The overflow discharge over the wing crest is described using the broad-crested weir equation:

$$q'_{over} = C_w \sqrt{2g} h_{pond}^{3/2} \tag{10}$$

where, C_w is the weir discharge coefficient; h_{pond} is the upstream ponding depth above the wing crest; g is the acceleration due to gravity. Eqs. (9) and (10) establish the relationship among runoff inflow, transverse seepage, and surface overflow. Thus, for a specified rainfall intensity, the seepage rate, overflow discharge, and ponding depth are determined from the coupled water-balance and hydraulic conditions rather than prescribed independently.

3.1.4 Longitudinal seepage within the bamboo wing

Water entering the bamboo bundle through the vegetation bag wall is transported longitudinally toward the Y-shaped junction. Because the bamboo wings are installed on an inclined slope, the longitudinal hydraulic gradient is governed jointly by the pressure-head gradient and the gravitational component. Let x denote the longitudinal coordinate measured from the wing tip toward the Y-shaped junction. The longitudinal seepage is described by Darcy's law using the total hydraulic gradient, which accounts for both the pressure-head and elevation gradients:

$$Q_x = -k_{long} A_{void} \left(\frac{dh}{dx} + \frac{dz}{dx} \right) \tag{11}$$

where, k_{long} is the longitudinal hydraulic conductivity of the bamboo bundle; Avoid is the effective void cross-sectional area of the bamboo bundle; h is the pressure head; z is the elevation head.

For a bamboo bundle with an effective porosity n, the effective void cross-sectional area is given by:

$$A_b = nA_{void} \tag{12}$$

where, A_b is the total cross-sectional area of the bamboo bundle.

The wing tip is assumed to be exposed to atmospheric pressure and is therefore taken as the reference hydraulic-head boundary. The boundary condition is expressed as:

$$h(0) = 0 \tag{13}$$

The longitudinal seepage solution is obtained by integrating along the wing, with the transverse seepage through the vegetation bag wall providing the distributed water input. The longitudinal seepage equation is solved iteratively together with the transverse seepage relation given in Section 3.1.5. The resulting pressure head at the Y-shaped junction, i.e., at $x=L_y$, is denoted by $h_{junction}$. This junction pressure head provides the hydraulic driving force for subsequent internal seepage through the central drainage stem.

3.1.5 Transverse seepage through the vegetation bag wall

The transverse seepage through the vegetation bag wall is governed by Darcy's law. The seepage rate per unit wing length is expressed as:

$$q_0 = \left(\frac{k_{bag} \Delta h}{\delta} \right) \left(H_{out} - H_{in} \right) \tag{14}$$

where, k_{bag} is the hydraulic conductivity of the vegetation bag wall; δ is the bag-wall thickness of the vegetation bag; W_{wet} is the wetted perimeter; H_{out} and H_{in} denote the hydraulic heads immediately outside and inside the vegetation bag wall, respectively. The hydraulic head difference is determined by the head differential between the exterior water level outside the vegetation bag and the internal pressure head within the bamboo bundle. Therefore, q_0 is determined from the hydraulic-head distribution rather than introduced as an independent empirical input. The calculated seepage rate is incorporated into the longitudinal seepage analysis to determine the pressure head at the Y-shaped junction. An iterative procedure is adopted to obtain a converged solution for the coupled seepage and overflow processes.

3.1.6 Flow partition at the bottom of the central drainage stem

At the Y-shaped junction, water transported through the two bamboo wings converges toward the central drainage stem. Meanwhile, rainfall directly received by the bamboo structure is divided between the external surface-flow and internal-seepage pathways. Accordingly, the total outflow from the structure is considered to consist of two parallel pathways: surface flow Q_1 and internal seepage Q_2.

Pathway 1: Surface flow:

The fraction of direct rainfall contributing to the external surface-flow pathway is expressed as:

$$Q_{direct,s} = CQ_{direct} \tag{15}$$

where, C is the surface-routing coefficient representing the fraction of direct rainfall routed along the external surface of the bamboo structure.

The total overflow discharge from the two bamboo wings is calculated as:

$$Q_{over} = 2L_y q'_{\text{over}} \tag{16}$$

where, q'_{over} is the overflow discharge per unit wing length obtained from the water-balance equation and the broad-crested weir equation.

The surface-flow discharge reaching the bottom of the central drainage stem is then expressed as:

$$Q_1 = Q_{over} + Q_{direct,s} \tag{17}$$

where, Q_1 represents the total surface-flow discharge.

Pathway 2: Internal seepage through the bamboo bundle:

The internal seepage discharge through the vertical bamboo rod driven by the hydraulic head developed at the Y-shaped junction is determined according to Darcy's law:

$$Q_{stem} = k_{stem} A_{void,stem} \frac{h_{junction}}{L_s} \tag{18}$$

where, Q_{stem} is the seepage discharge through the central drainage stem driven by the hydraulic head at the Y-shaped junction; k_{stem} is the effective hydraulic conductivity of the central drainage stem; $A_{void,stem}$ is the effective void cross-sectional area of the central drainage stem, $h_{junction}$ is the pressure head at the Y-shaped junction; L_S is the length of the central drainage stem.

The effective void cross-sectional area of the central drainage stem is determined from its cross-sectional geometry and effective porosity as:

$$A_{void,stem} = n_s A_s \tag{19}$$

where, n_s is the effective porosity of the central drainage stem; A_s is the total cross-sectional area of the central drainage stem.

The total internal-seepage discharge Q_2 therefore comprises the flow transported from the bamboo wings and the fraction of direct rainfall entering the internal pathway:

$$Q_2 = Q_{stem} + (1-C)Q_{direct} \tag{20}$$

where, the first term represents seepage transported from the wings through the Y-shaped junction, whereas the second term represents direct rainfall entering the internal pathway.

3.1.7 Summary of theoretical interception under the representative operating condition

Based on the parallel-flow-path framework described above, the theoretical runoff interception performance of the Y-shaped bamboo structure is determined from the combined surface-flow and internal-seepage pathways. The total water discharge collected at the bottom outlet is therefore obtained by summing the two flow components:

$$Q_{total} = Q_1 + Q_2 \tag{21}$$

The calculated outlet discharge represents the total water routed through the Y-shaped bamboo structure under the specified rainfall and geometric conditions. The model was subsequently validated against the indoor flume-test results to evaluate its predictive capability.

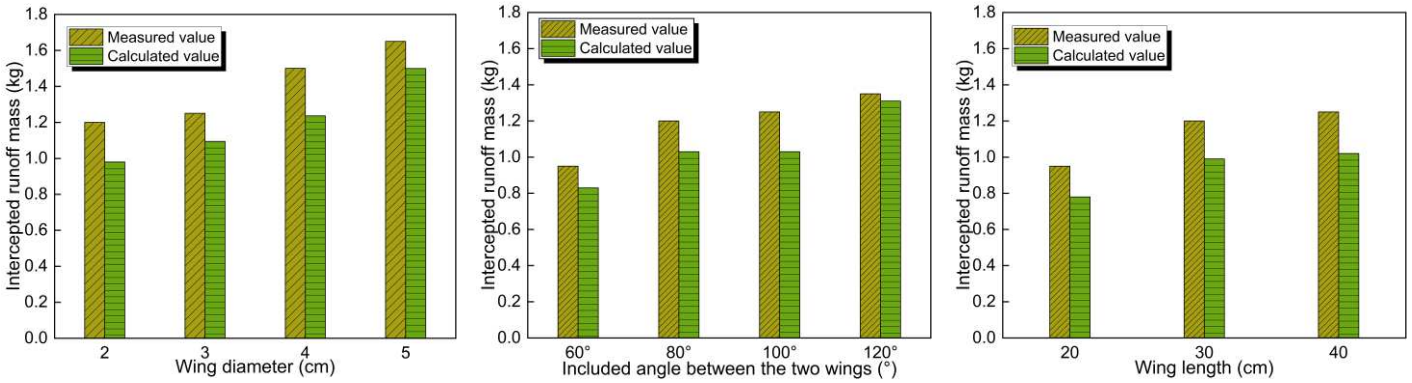
3.2 Model validation

To evaluate the predictive performance of the proposed theoretical model, it was applied to reproduce the results of the indoor model tests using the experimentally measured parameters. The model inputs were set as follows: I=0.10 g/(cm²·min), T=10 min, d=4 cm, δ=0.086 cm, k_{bag}=0.042 cm/s, k_{long}=0.1 cm/s, φ=21.8°. The geometric parameters of the Y-

shaped members are consistent with those used in the indoor flume tests, with θ=80°, L_y=30 cm, d_y=3 cm, H_{up}=13 cm, d_s=4 cm, L_s=30 cm.

Figure 6 compares the measured and predicted results. The theoretical predictions generally reproduce the trend of the experimental measurements, although a systematic underestimation is observed. This discrepancy is mainly attributed to the simplified treatment of the contributing water sources and flow processes. Specifically, the present formulation considers the upstream contributing area but does not explicitly account for lateral inflow from the outer sides of the wing rods, splash-induced water supply, or additional interception associated with flow diversion around the rods. These effects may increase the effective water supply to or interception effectiveness of the structure, thereby contributing to the higher interception observed experimentally. Incorporating these mechanisms into the theoretical framework may further improve its predictive accuracy.

The overall prediction performance is quantified by the error statistics presented in Table 3. The mean absolute error (MAE) is approximately 0.17 kg, the mean absolute percentage error (MAPE) is approximately 11.5%, and the coefficient of determination (R^2) is greater than 0.90. The high R^2 indicates a strong correspondence between the predicted and measured values, while the relatively low MAE and moderate MRE indicate that the model captures the overall variation in the measured response reasonably well despite the observed systematic underestimation.



(a) Comparative results on the impact of wing diameter (b) Comparative results on the impact of included angle (c) Comparative results on the impact of wing length

Figure 6. Comparison of measured and predicted results.

Table 3. Global error indicators for model validation.

Indicator	Value	Evaluation criterion	Grade
Mean Squared Error (MSE)	0.043229 kg²	—	—
Root Mean Squared Error (RMSE)	0.2079 kg	—	—
Mean Absolute Error (MAE)	0.1731 kg	—	—
Mean Absolute Percentage Error (MAPE)	11.54%	10%–20% [25]	Good
Correlation coefficient (R)	0.9534	$\|R\| \geq 0.90$	Very strong
Coefficient of determination (R^2)	0.9090	$R^2=(0.9534)^2$	—
Nash–Sutcliffe efficiency (NSE)	0.7046	0.65–0.75 [26]	Good
Normalized RMSE by mean (CV-RMSE)	12.63%	10%–20%	Good

4. Discussion

The experimental and theoretical results demonstrate that the Y-shaped bamboo structure can effectively intercept and regulate surface runoff through its coupled geometric and hydraulic characteristics. As a natural biomass material, bamboo also offers advantages in terms of strength-to-weight ratio, ease of processing, and environmental compatibility, supporting its potential application in ecological slope protection[27,28]. However, the durability of bamboo-based structures remains an important consideration for long-term field application. The accelerated aging tests showed that the runoff interception efficiency decreased by approximately 4% after 30 combined drying-wetting and freeze-thaw

cycles, while the basic interception function was retained. This moderate reduction indicates that repeated environmental exposure can progressively affect the hydraulic performance of the structure. Repeated drying and wetting may induce cyclic swelling and shrinkage of bamboo tissues, potentially altering the continuity of internal flow pathways and the contact conditions between bamboo elements[29]. Freeze-thaw cycling may further promote microstructural damage through repeated water-ice phase transitions and weaken the confinement provided by the vegetation bag[30]. These processes may collectively modify the storage and conveyance characteristics of the bamboo bundle, thereby reducing its effective runoff interception capacity. Nevertheless, the present tests were conducted under controlled laboratory conditions and primarily represent a short-term degradation tendency. The observed 4% reduction should therefore not be directly interpreted as a field-scale service-life attenuation rate, because natural exposure also involves ultraviolet radiation, microbial activity, seasonal moisture fluctuations, and other environmental factors[31,32].

Moreover, the present erosion tests were conducted on a relatively small acrylic slope with a fixed gradient of 1:2.5, which provided well-controlled conditions for isolating the effects of structural parameters but does not fully reproduce the hydraulic and soil conditions of natural slopes. Natural slopes are characterized by heterogeneous soil properties, surface roughness, preferential flow paths, vegetation, and spatial variations in moisture content, all of which can modify runoff generation and infiltration. In addition, slope gradient can alter runoff velocity, hydraulic shear stress, and the conditions for ponding and overflow[33]. Therefore, the geometric parameters optimized under the present conditions should not be regarded as universal design values for all slope configurations. The relatively small flume dimensions (70 cm×70 cm) may also have introduced sidewall effects by restricting lateral runoff spreading and modifying flow convergence toward the Y-shaped structure[34]. Accordingly, the present results should be regarded as a mechanistic and experimental basis for the design of Y-shaped bamboo structures rather than a direct field-design criterion. Future investigations should evaluate a broader range of rainfall intensities, slope gradients, slope lengths, and soil types using larger-scale models and natural rainfall conditions. Long-term field monitoring combined with multi-factor aging tests will also be required to quantify durability-related performance attenuation and establish appropriate correction factors for practical engineering design.

5. Conclusions

This study proposed and experimentally evaluated an ecological slope protection technique based on a Y-shaped bamboo structure, and developed a coupled theoretical model to interpret its runoff interception mechanisms. The main conclusions are summarized as follows:

(1) The cumulative runoff interception of the Y-shaped bamboo structure increased nearly linearly with rainfall duration. Compared with solid wood components, the Y-shaped structure consistently exhibited higher interception efficiency, highlighting the potential of bamboo as a sustainable material for ecological slope protection.

(2) The sensitivity of interception efficiency to geometric parameters followed the order: included angle > wing length > wing diameter. These three parameters together accounted for 93.04% of the total variance, indicating that the macroscopic geometric configuration was the dominant factor governing interception efficiency.

(3) A theoretical runoff interception model coupling weir flow theory with Darcy's law was established and validated against laboratory model tests, demonstrating satisfactory predictive performance. The model provides an effective predictive framework and theoretical basis for the design and optimization of bamboo-based runoff interception structures for ecological slope protection.

References

1. Gu, X., Song, L., Xia, X. & Yu, C. Finite element method-peridynamics coupled analysis of slope stability affected by rainfall erosion. Water 16, 2210 (2024).
2. Tao, H., Lei, S. W., Gong, L., Shi, X., Zhang, M. M. & Yang, G. Q. Study on erosion and stability of the ecological slope. Front. Earth Sci. 10, 1071231 (2023).
3. Cheng, Q., Hou, K., Sun, H. & Niu, X. Numerical simulation of rainfall-induced erosion on infiltration and slope stability. Water 16, 1517 (2024).
4. Wang, F., Dai, Z., Takahashi, I. & Tanida, Y. Soil moisture response to water infiltration in a 1-D slope soil column model. *Eng. Geol.* **267**, 105482 (2020).
5. Zhang, Z., Zeng, R., Meng, X., Zhao, S., Wang, S., Ma, J. & Wang, H. Effects of changes in soil properties caused by progressive infiltration of rainwater on rainfall-induced landslides. *Catena* **233**, 107475 (2023).
6. Vivoda Prodan, M., Peranić, J., Pajalić, S. & Arbanas, Ž. Physical modelling of rainfall-induced sandy and clay-like slope failures. *Adv. Mater. Sci. Eng.* **2023**, 3234542 (2023).

7. Zhao, N., Lu, H. & Zhang, R. The coupling effect of pore water pressure and pore water gravity in unsaturated soils under rainfall condition and its influence on slope stability. *Geofluids* **2022**, 9492514 (2022).
8. Liu, S., Yin, K., Du, J., Chen, L., Xie, X., Zhu, S. & Zhang, X. Landslides triggered by the extreme rainfall on July 4, 2023, Wanzhou, China. *Landslides* **22**, 2935–2947 (2025).
9. Whitman, J. B., Schussler, J. C., Perez, M. A. & Liu, L. Hydraulic performance evaluation of wattles used for erosion and sediment control. *J. Irrig. Drain. Eng.* **147**, 04021028 (2021).
10. Babur, E., Kara, O., Fathi, R. A., Susam, Y. E., Riaz, M., Arif, M. & Akhtar, K. Wattle fencing improved soil aggregate stability, organic carbon stocks and biochemical quality by restoring highly eroded mountain region soil. *J. Environ. Manage.* **288**, 112489 (2021).
11. Kincl, D., Kabelka, D., Heřmanovská, D., Vopravil, J., Urban, R. & Křemen, T. Evaluation of sediment barriers in relation to the trap of soil particles. *Soil Water Res.* **17**, 201 (2022).
12. Donald, W. N., Zech, W. C. & Fang, X. Comparative evaluation of wattle ditch checks composed of differing materials and properties. *J. Irrig. Drain. Eng.* **141**, 04014051 (2015).
13. Robichaud, P. R., Pierson, F. B., Brown, R. E. & Wagenbrenner, J. W. Measuring effectiveness of three postfire hillslope erosion barrier treatments, western Montana, USA. *Hydrol. Process.* **22**, 159–170 (2008).
14. Sari, P. T. K., Mochtar, I. B. & Chaiyaput, S. Effectiveness of horizontal sub-drain for slope stability on crack soil using numerical model. *Geotech. Geol. Eng.* **41**, 4821–4844 (2023).
15. Abed, M., Peethambaran, B. & Leshchinsky, B. Evaluating transient drawdown and slope stabilization from horizontal drain installation. *Comput. Geotech.* **167**, 106044 (2024).
16. Zhang, X., Wang, H., Gao, Z., Xiang, K., Zhai, Q., Satyanaga, A. & Chua, Y. S. Evaluation of the performance of the horizontal drain in drainage of the infiltrated water from slope soil under rainfall conditions. *Sustainability* **15**, 14163 (2023).
17. Parhizkar, M., Shabanpour, M., Lucas-Borja, M. E., Zema, D. A., Li, S., Tanaka, N. & Cerda, A. Effects of length and application rate of rice straw mulch on surface runoff and soil loss under laboratory simulated rainfall. *Int. J. Sediment Res.* **36**, 468–478 (2021).
18. Díaz, M. G., Lucas-Borja, M. E., Gonzalez-Romero, J., Plaza-Alvarez, P. A., Navidi, M., Liu, Y. F., Wu, G. L. & Zema, D. A. Effects of post-fire mulching with straw and wood chips on soil hydrology in pine forests under Mediterranean conditions. *Ecol. Eng.* **182**, 106720 (2022).
19. Wang, C., Ma, J., Wang, Y., Li, Z. & Ma, B. The influence of wheat straw mulching and straw length on infiltration, runoff and soil loss. *Hydrol. Process.* **36**, e14561 (2022).
20. Won, C. H., Shin, M. H., Choi, Y. H., Shin, J. Y., Park, W. J. & Choi, J. D. Simulations of runoff using rice straw mats and soil amendments. *J. Korean Soc. Agric. Eng.* **54**, 95–102 (2012).
21. Guo, C., Zhao, Q., Wu, J., Li, H., Yang, H. & Wu, Z. Permeability prediction in geotextile envelope after chemical clogging: A coupled model. *Geotext. Geomembr.* **50**, 1172–1187 (2022).
22. Tian, J., Liu, S., Lu, Y., Cao, R., Zhang, Y. & Hu, Y. Hydraulic conductivity characteristics of woven geotextiles used in geotextile sand containers: Experimental investigation and a predictive model. *Ocean Eng.* **354**, 125047 (2026).
23. Vega-Garcia, P., Schwerd, R., Scherer, C., Schwitalla, C. & Helmreich, B. Development of a model for stormwater runoff prediction on vertical test panels coated with plaster and mortar. *Water* **12**, 2593 (2020).
24. Grasso, M., Rivera, Y., Petrov, V. & Manera, A. Experimental measurements and multiphase CFD simulations of thin flowing films down an inclined plate with demonstration of proof of principle innovative method for velocity profile reconstruction in thin films. *Nucl. Eng. Des.* **451**, 114829 (2026).
25. Lewis, C. D. *Industrial and Business Forecasting Methods: A Practical Guide to Exponential Smoothing and Curve Fitting*. Butterworth Scientific, London (1982).
26. Moriasi, D. N., Arnold, J. G., Van Liew, M. W., Bingner, R. L., Harmel, R. D. & Veith, T. L. Model evaluation guidelines for systematic quantification of accuracy in watershed simulations. *Trans. ASABE* **50**, 885–900 (2007).
27. Kumar, D. & Mandal, A. Review on manufacturing and fundamental aspects of laminated bamboo products for structural applications. *Constr. Build. Mater.* **348**, 128691 (2022).
28. Adier, M. F. V., Sevilla, M. E. P., Valerio, D. N. R. & Ongpeng, J. M. C. Bamboo as sustainable building materials: A systematic review of properties, treatment methods, and standards. *Buildings* **13**, 2449 (2023).
29. Mou, Q., Hao, X., Xu, K., Li, X. & Li, X. Hygroexpansion behaviors of bamboo in response to moisture absorption and desorption. *Constr. Build. Mater.* **341**, 127895 (2022).
30. Gan, J., Zhang, Y., Lin, Q. & Yu, W. Moisture-mediated freeze-thaw degradation in bamboo from cellulose hydration to macroscale fracture. *Carbohydr. Polym.* **366**, 123884 (2025).
31. Rao, F., Li, X., Li, N., Li, L., Liu, Q., Wang, J., Zhu, X. & Chen, Y. Photodegradation and photostability of bamboo: Recent advances. *ACS Omega* **7**, 24041 (2022).
32. Li, H., Liu, Y., Wu, Y., Dauletbek, A., Duan, Y. & Corbi, O. The aging behavior of Moso bamboo in natural weathering condition. *Ind. Crops Prod.* **222**, 119901 (2024).
33. Zhang, K., Xu, X., Iversen, B. V., Weber, P. L., de Jonge, L. W., Wang, X. & Bai, Y. Effect of different underlying surfaces on hydraulic parameters of overland flow. *Soil Tillage Res.* **232**, 105776 (2023).
34. Tian, Y., Xu, Y., Yang, M., Jiang, F., Zhang, Y., Huang, Y. & Lin, J. Effect of flume width on the hydraulic properties of overland flow from laboratory observation. *Water* **15**, 3416 (2023).

Acknowledgements

Funding: This study is supported by Jiangsu Provincial Department of Transportation (2025QD06) and Jiangsu Provincial University-Industrial Research Collaboration Project (BY20221035).

Author Contributions statement

X.Y.: conceptualization; investigation; funding acquisition. Q.L.: methodology; data curation. W.X.: conceptualization; writing—original draft. Z.C.: writing—review & editing. C.L.: supervision; validation. C.C.: supervision; conceptualization. All authors have read and agreed to the published version of the manuscript.

Data Availability Statement

Data will be made available on request.

Conflicts of Interest

The authors declare no conflicts of interest.